Fano-type interference in quantum dots coupled between metallic and superconducting leads

Jan Barański and T. Domański
Institute of Physics, Maria Curie-Skłodowska University, PL-20-031 Lublin, Poland
(Received 21 July 2011; revised manuscript received 24 September 2011; published 7 November 2011)

We analyze the quantum interference effects appearing in the charge current through the double quantum dots coupled in T-shape configuration to an isotropic superconductor and metallic lead. Owing to the proximity effect the quantum dots inherit a pairing which has a profound influence on nonequilibrium charge transport, especially in the subgap regime $|V| < \Delta/|e|$. We discuss under what conditions the Fano-type line shapes might appear in such Andreev conductance and consider a possible interplay with the strong correlation effects.

DOI: 10.1103/PhysRevB.84.195424 PACS number(s): 73.63.Kv, 73.23.Hk, 74.45.+c, 74.50.+r

I. INTRODUCTION

Heterostructures with nano-objects (such as quantum dots, nanowires, molecules, etc.) hybridized to one conducting and another superconducting electrode seem to be promising testing fields where strong electron correlations (responsible, e.g., for Coulomb blockade and Kondo physics[1]) can be confronted with the superconducting order.[2] Coulomb repulsion between electrons in solid-state physics is known to suppress local (s-wave) pairing and, through a spin-exchange mechanism, eventually promotes intersite (d-wave) superconductivity.[3] A mutual relation between such repulsion and the local pairing is, however, rather difficult to study, both on theoretical grounds and experimentally. In nanoscopic heterostructures some of these limitations can be overcome by a flexible adjustment of the hybridization and gate-voltage positioning of the energy levels involved in the charge transfer[4] enabling a controllable changeover between the Kondo regime and the opposite case dominated by the induced on-dot pairing.

Quantum dots (QDs) coupled with strength Γ_N to metallic conductor (N) and with Γ_S to superconducting electrode (S) can exhibit features characteristic to both on-dot pairing and the Kondo effect, including their coexistence.[5] Their efficiency depends on the ratio Γ_S/Γ_N. In the limit $\Gamma_S \gg \Gamma_N$ the underlying physics is controlled by on-dot pairing and manifests itself, e.g., by particle-hole splitting of the quasiparticle levels. On the other hand, for $\Gamma_S \ll \Gamma_N$ strong correlations take over (the Kondo effect appears for sufficiently low temperatures $T < T_K$). Nontrivial aspects related to such interplay between Coulomb interactions and proximity-induced on-dot pairing has been addressed theoretically using various methods such as the mean-field slave-boson approach,[6] noncrossing approximation,[7] perturbative scheme,[2,8] constrained slave-boson technique,[9] numerical renormalization group,[10–12] and others.[13–16] In addition, the cotunneling regime of a Coulomb blockaded quantum dot sandwiched between a normal and superconducting lead, where charge fluctuations are strongly suppressed, has been discussed emphasizing the role of in-gap resonances.[17]

As far as the experimental situation is concerned, it has been less intensively explored. The earliest transport measurements for N-QD-S interface have been obtained using a multiwall carbon nanotube deposited between Au and Al electrodes.[18] Such investigations concentrated, however, on the specific regime $k_B T_K \geqslant \Delta$, when the correlations dominated over the proximity effect. Other studies of the same group have been done for similar structures, replacing a metallic electrode by a ferromagnet.[19] Several recent efforts focused on multiterminal structures involving two normal electrodes and one superconducting electrode as potential scenarios for the realization of crossed Andreev reflections tunable via gate voltages,[20] Cooper pair splitters,[21] and QD spin valves.[22]

Valuable understanding of a subtle interplay between the correlations and the induced on-dot pairing has been gained from recent measurements by Deacon *et al.*[5] The authors have explored a subgap transport originating from Andreev-type scattering processes for several representative ratios Γ_S/Γ_N using self-assembled InAs quantum dots deposited between the gold (N) and aluminum (S) electrodes. Their measurements provided unambiguous experimental evidence for (a) particle-hole splitting of the Andreev states in the subgap conductance for $\Gamma_S \geqslant \Gamma_N$ and (b) enhancement of the zero-bias Andreev conductance due to formation of Kondo resonance at the Fermi level of metallic lead, as has been qualitatively suggested by our studies[16] and also indicated by other groups.[23] Recently, in-gap Andreev bound states have also been experimentally observed in the nanostructures with carbon nanotubes spread between two superconducting leads.[24] This very interesting aspect is related to dc Josephson supercurrent transmitted via the proximity-induced Andreev bound states.

In this work we extend our studies of the Andreev conductance,[16] taking into account the quantum interference effects due to additional degrees of freedom involved in the charge transport. As the simplest prototype for the Fano-type interference[25] we consider the setup (see Fig. 1) with a side-attached quantum dot contributing an extra pathway for electrons transmitted between the metallic and superconducting leads. Our analysis can be regarded as complementary to the study by Tanaka *et al.* who considered double quantum dots coupled between N and S leads in the T-shape setup (assuming $U_1 = 0$, $U_2 \neq 0$)[26] and the series configuration.[27]

In Sec. II we introduce the microscopic model and briefly outline basic notes on nonequilibrium subgap transport. In Sec. III we discuss a unique way in which the Fano-type line shapes can be observed in the Andreev conductance, focusing on the uncorrelated quantum dots. In the final sections we discuss the influence of correlations at the interfacial quantum dot (Sec. IV) and the side-attached one (Sec. V). We end with a summary and suggestions for future studies.

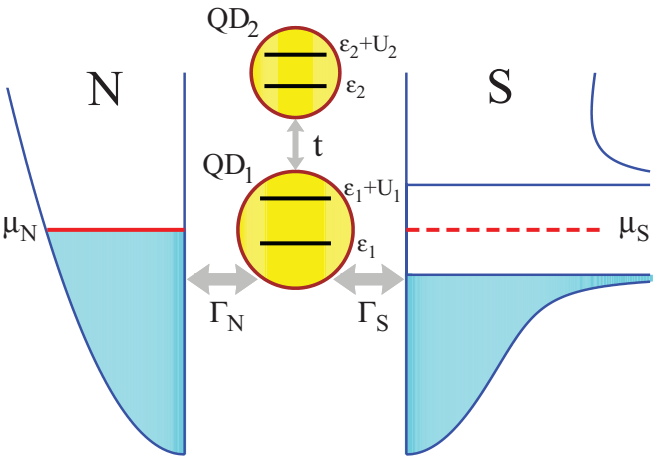

FIG. 1. (Color online) Scheme of the double quantum dot in T-shape configuration coupled to the conducting (N) and superconducting (S) leads, where interference effects originate from the interdot hopping t.

II. THE MODEL

For a description of the heterojunction sketched in Fig. 1 we use the following Hamiltonian:

$$\hat{H} = \hat{H}_N + \hat{H}_{N\text{-DQD}} + \hat{H}_{\text{DQD}} + \hat{H}_{S\text{-DQD}} + \hat{H}_S. \tag{1}$$

The double quantum dot (DQD) is represented by

$$\hat{H}_{\text{DQD}} = \sum_{\sigma i} \varepsilon_i \hat{d}^\dagger_{i\sigma}\hat{d}_{i\sigma} + \sum_{\sigma}(t\ \hat{d}^\dagger_{1\sigma}\hat{d}_{2\sigma} + \text{H.c.}) + \sum_i U_i\ \hat{n}_{i\uparrow}\hat{n}_{i\downarrow}, \tag{2}$$

where energies of each ($i = 1,2$) quantum dot electron are denoted by ε_i and t stands for the interdot hopping. Besides considering the interference effects for the noninteracting case we also try to investigate the influence of correlations caused by the Coulomb repulsion U_i between opposite spin electrons $\sigma = \uparrow, \downarrow$ at the interfacial $i = 1$ (Sec. IV) and the side-coupled $i = 2$ (Sec. V) quantum dots.

The external reservoirs N and S of charge carriers are described by $\hat{H}_N = \sum_{\mathbf{k},\sigma} \xi_{\mathbf{k}N}\hat{c}^\dagger_{\mathbf{k}\sigma N}\hat{c}_{\mathbf{k}\sigma N}$ and correspondingly, $\hat{H}_S = \sum_{\mathbf{k},\sigma} \xi_{\mathbf{k}S}\hat{c}^\dagger_{\mathbf{k}\sigma S}\hat{c}_{\mathbf{k}\sigma S} - \sum_{\mathbf{k}} \Delta\hat{c}^\dagger_{\mathbf{k}\uparrow S}\hat{c}^\dagger_{-\mathbf{k}\downarrow S} + \Delta^*\hat{c}_{-\mathbf{k}\downarrow S}\hat{c}_{\mathbf{k}\uparrow S}$ assuming the isotropic energy gap Δ. As usual, $\xi_{\mathbf{k}\beta} = \varepsilon_{\mathbf{k}\beta} - \mu_\beta$ denotes the electron energies measured from the individual chemical potentials μ_β which become detuned $\mu_N - \mu_S = eV$ if a bias V is applied across the junction inducing the nonequilibrium charge flow $I(V)$. The Fano-type quantum interference effects, originating from the hopping t to side-coupled quantum dot, shall be discussed assuming that only the interfacial quantum dot $i = 1$ is directly coupled to the external leads

$$\hat{H}_{\beta\text{-DQD}} = \sum_{\mathbf{k},\sigma}(V_{\mathbf{k}\beta}\hat{d}^\dagger_{1\sigma}\hat{c}_{\mathbf{k}\sigma\beta} + \text{H.c.}). \tag{3}$$

In the wide-band limit approximation it is convenient to introduce the structureless coupling constants $\Gamma_\beta = 2\pi\sum|V_{\mathbf{k}\beta}|^2\delta(\omega - \xi_{\mathbf{k}})$ which shall be used here as the energy units.

Interplay between the proximity-induced on-dot pairing, the correlations, and the quantum interference effects can in practice be detected by measuring the differential conductance $dI(V)/dV$. Particularly valuable for this purpose is the low-voltage (subgap) regime $|eV| \ll \Delta$. Under such conditions the charge current is provided by the anomalous Andreev scattering in which electrons from the metallic lead are converted into Cooper pairs in superconductors with a simultaneous reflection of the electron holes back to the normal lead. On a formal level the resulting Andreev current can be expressed by the following Landauer-type formula:[9,13]

$$I_A(V) = \frac{2e}{h}\int d\omega\, T_A(\omega)[f(\omega - eV,T) - f(\omega + eV,T)], \tag{4}$$

where $f(\omega,T)$ is the Fermi distribution function and the transmittance $T_A(\omega) = \Gamma_N^2|G_{1,12}(\omega)|^2$ depends on the off-diagonal part (in the Nambu notation) of the retarded Green's function $\boldsymbol{G}_1$ of the interfacial quantum dot (5).

III. FANO RESONANCES

Fano-type resonances appear in many physical systems due to quantum interference of the waves transmitted resonantly via some discrete energy level combined with a transmittance contributed from a continuum of other states. In nanoscale physics such resonances take place in a variety of constructions.[25] Fano line shapes have been observed, for instance, in scanning tunneling microscope images of Co adatoms deposited on metallic surfaces[30,31] and have been theoretically described using magnetic impurity models.[32,33] Similar effects can also be seen in electron transport, when external electrodes are coupled in parallel through a quantum dot and directly via a shortcut bridge.[28,29] Another possibility occurs in electron tunneling using two quantum dots of considerably different line broadenings.[34,35] In the latter case the narrower level is responsible for forming the Fano resonance on a background of the broader level.

In this work we analyze similar interference effects appearing in the anomalous Andreev current, which is very specific because of the particle and hole degrees of freedom mixed with one another. To have a clear picture of the underlying physics let us start by considering the noninteracting case $U_i = 0$ when the Green's functions of each quantum dot can be determined exactly.

Electron transport of the setup shown in Fig. 1 is determined by effective properties of the interfacial quantum dot. For this purpose we compute the matrix Green's function $\boldsymbol{G}_1(t',t_0) = -i\hat{T}\langle\hat{\Psi}_1(t')\hat{\Psi}_1^\dagger(t_0)\rangle$ introducing the standard spinor notations $\hat{\Psi}_1^\dagger = (\hat{d}^\dagger_{1\uparrow},\hat{d}_{1\downarrow})$ and $\hat{\Psi}_1 = (\hat{\Psi}_1^\dagger)^\dagger$. In the equilibrium condition $\mu_N = \mu_S$ this function depends only on the time difference and its Fourier transform obeys the following Dyson equation:

$$\boldsymbol{G}_1(\omega)^{-1} = \begin{pmatrix}\omega - \varepsilon_1 & 0\\ 0 & \omega + \varepsilon_1\end{pmatrix} - \boldsymbol{\Sigma}_1^0(\omega) - \boldsymbol{\Sigma}_1^U(\omega), \tag{5}$$

where the term $\boldsymbol{\Sigma}_1^0(\omega)$ corresponds to the self-energy of noninteracting case ($U_1 = 0$) and $\boldsymbol{\Sigma}^U(\omega)$ accounts for the correlation effects (discussed in Sec. IV). Focusing on the

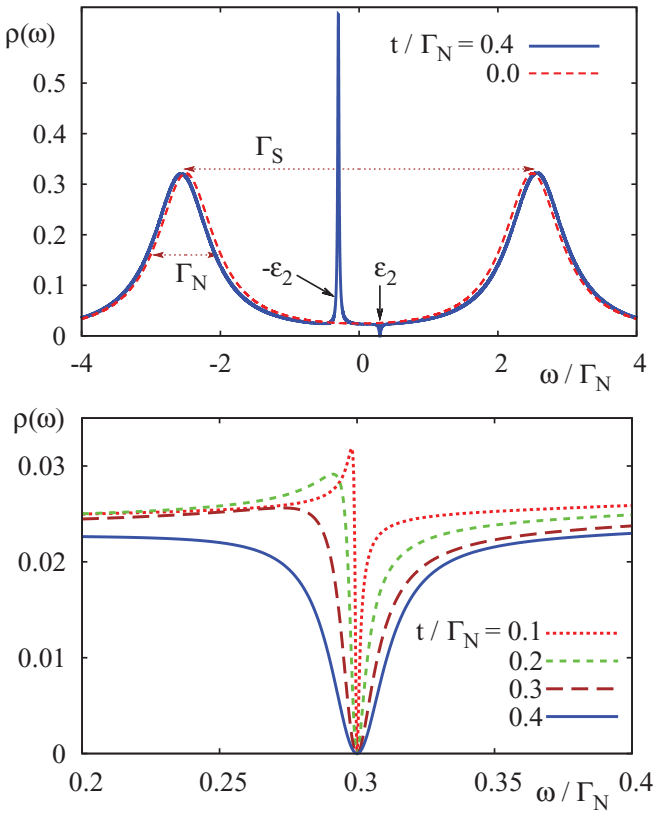

FIG. 2. (Color online) Density of states $\rho(\omega)$ of the interfacial $i = 1$ QD obtained in equilibrium conditions for $\varepsilon_1 = 0$, $\varepsilon_2 = 0.3\Gamma_N$, $\Gamma_S = 5\Gamma_N$, and a few values of the interdot hopping t.

deep subgap regime $|\omega| \ll \Delta$ we find that $\mathbf{\Sigma}_1^0(\omega)$ is given by (see Appendix A)

$$\mathbf{\Sigma}_1^0(\omega) = \begin{pmatrix} -\frac{i\Gamma_N}{2} + \frac{t^2}{\omega-\varepsilon_2} & -\frac{\Gamma_S}{2} \\ -\frac{\Gamma_S}{2} & -\frac{i\Gamma_N}{2} + \frac{t^2}{\omega+\varepsilon_2} \end{pmatrix}. \tag{6}$$

When the interference effects caused by the hopping t to the side-coupled QD are neglected the expression (6) becomes static (ω independent) and nontrivial physics of this, so-called *atomic superconducting limit*, has been explored in detail by several groups,[2,10,36] including ourselves.[16]

Taking into account quantum interference $t \neq 0$, in Fig. 2 we show the energy spectrum $\rho(\omega) = -\frac{1}{\pi}\mathrm{Im}\,\boldsymbol{G}_{1,11}(\omega + i0^+)$ manifesting the proximity-induced on-dot pairing [formally arising from the off-diagonal parts of Eq. (6)] obtained for strong coupling to the superconducting lead $\Gamma_S = 5\Gamma_N$. The coupling Γ_S is responsible for the particle-hole splitting of the effective quasiparticle states formed at $\pm\sqrt{\varepsilon_1^2+(\Gamma_S/2)^2}$, whereas the coupling Γ_N controls their broadening. In the particular case $\varepsilon_1 = 0$, the quasiparticle peaks appearing at $\pm E_1$ [where $E_1 \equiv \sqrt{\varepsilon_1^2+(\Gamma_S/2)^2}$] are symmetric, but for arbitrary ε_1 they are weighted by the corresponding BCS coefficients $u^2, v^2 = \frac{1}{2}(1 \pm \varepsilon_1/E_1)$.[16] On top of such behavior we clearly notice that hopping to the side-coupled quantum dot induces additional features appearing in the effective spectrum as the Fano resonance and antiresonance near $\pm\varepsilon_2$. For the case with both metallic leads just the single Fano structure at ε_2 would survive, which in a very pedagogical way has been discussed by Žitko.[34]

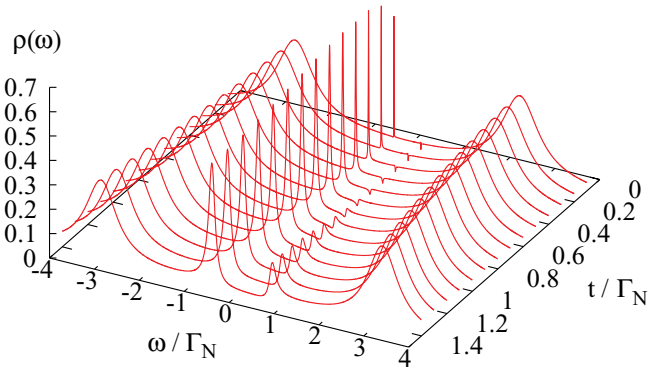

FIG. 3. (Color online) Changeover of the interfacial quantum dot spectrum from the Fano (resonance and antiresonance) line shapes to the effective four-peak structure upon increasing the interdot hopping t for the same parameters as in Fig. 2.

Fano-type line shapes (see the lower panel in Fig. 2) are present only in the weak hopping regime $t \ll \Gamma_N$. For increasing t the Fano structures gradually evolve into separate quasiparticle peaks, illustrated in Fig. 3. Physically this can be assigned to the induced pairing on the side-attached QD $\langle \hat{d}_{2\downarrow}\hat{d}_{2\uparrow}\rangle \neq 0$ transmitted there indirectly via the interfacial quantum dot. Such an effect again qualitatively differs from the structures of the DQD coupled to both metallic leads.[34,35]

Interrelation between the interference and proximity effect can be practically investigated by measuring the tunneling current. In Fig. 4 we show bias voltage V dependence of the differential Andreev conductance $G_A(V) = dI_A(V)/dV$ determined at zero temperature from Eq. (4) over a broad regime covering both the subgap quasiparticle peaks. Figure 5 illustrates the resulting Fano-type line shapes $G_A = G_0\frac{(x+q)^2}{x^2+1} + G_1$ nearby $-\varepsilon_2$, where $x = |eV + \varepsilon_2|/\Gamma_N$ and the asymmetry parameter q gradually decreases upon increasing the hopping integral t. Our results can be thought of as an extension of the predictions obtained for the normal electron tunneling using the T-shape DQD coupled to both metallic leads[34,38] onto the anomalous Andreev current where particle-hole mixing plays an essential role.

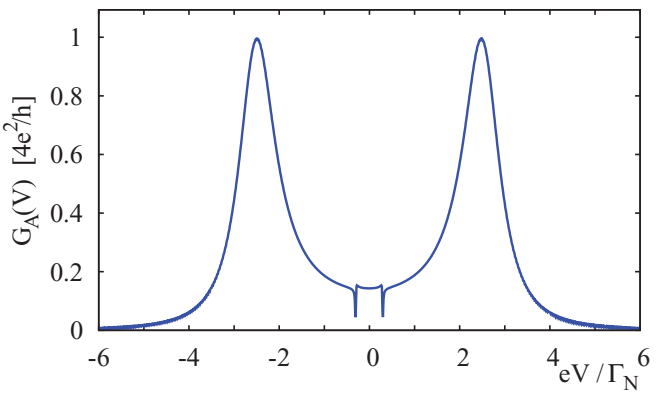

FIG. 4. (Color online) The differential Andreev conductance $G_A(V)$ versus the bias V revealing quasiparticle peaks [near $\pm\sqrt{\varepsilon_1^2 + (\Gamma_S/2)^2}$] and Fano-type line shapes (near $\pm\varepsilon_2$) for the set of parameters used in Fig. 2 and $t = 0.1\Gamma_N$.

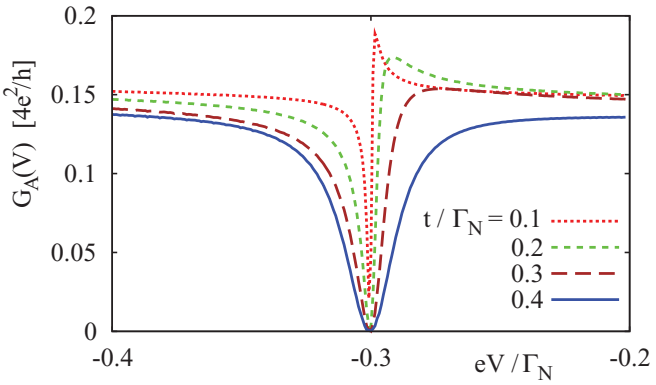

FIG. 5. (Color online) Differential conductance $G_A(V)$ of the subgap Andreev current versus the source-drain bias V in the vicinity of the Fano structure appearing at $V = \pm\varepsilon_2/e$.

IV. INTERPLAY WITH CORRELATIONS

Coulomb repulsion between electrons of opposite spins can have an important influence on the spectral and transport properties of various nanostructures. For the case of quantum dots coupled to both conducting leads such interactions are known to be responsible for (a) the charging effect (if a given energy level ε_i is attempted to be occupied by more than a single electron this costs the system an extra energy U_i) and (b) the Kondo effect when the singlet state is formed between QD and itinerant electrons from the leads.[37] In spectroscopic properties they are manifested by the appearance of a Coulomb satellite around $\omega = \varepsilon_i + U_i$ and a narrow Kondo resonance at the Fermi level. For heterostructures with superconducting electrodes the situation is more complex due to a competition between the induced on-dot pairing and Coulomb repulsion.

The rich interplay between the quantum interference, correlations, and proximity effect for the configuration shown in Fig. 1 have so far been addressed using the density functional technique[39] (which does not capture the Kondo physics) and by numerical renormalization-group calculations.[26] In the latter case the authors focused on $U_1 = 0$, $U_2 \neq 0$ when the side-attached quantum dot indirectly forms the Kondo state with electrons of the metallic lead thereby affecting the Andreev transport.

To account for the correlations U_1 originating from the interfacial quantum dot we extend the procedure previously used by us for studying the single quantum dot.[16] The main idea relies on choosing the matrix self-energy $\mathbf{\Sigma}_1^U(\omega)$ in a diagonal form

$$\mathbf{\Sigma}_1^U(\omega) \simeq \begin{pmatrix} \Sigma_N^{\mathrm{QD1}}(\omega) & 0 \\ 0 & -\left[\Sigma_N^{\mathrm{QD1}}(-\omega)\right]^* \end{pmatrix}. \tag{7}$$

Such a constraint (7) has been previously suggested in the numerical renormalization-group studies of the single QD coupled to N and S leads.[10] Formally, Eq. (7) can be regarded as the simplest guess for the unknown many-body self-energy $\mathbf{\Sigma}_1^U(\omega)$. As far as its physical aspects are concerned, by imposing the diagonal structure (7) we neglect any influence of the correlations U_1 on the induced on-dot pairing. It seems that for the limit $\Delta \gg \Gamma_\beta$ studied here, such an approximation might be justified. Partial confidence is also provided by the fairly good qualitative agreement between our former studies[16] based on Eq. (7) and the experimental data[5] obtained for InAs quantum dots on the interface between N and S leads. In more sophisticated treatments one should of course consider a possible influence of the correlations U_1 on off-diagonal channels of the matrix $\mathbf{\Sigma}_1^U(\omega)$. We hope that using approximation (7) we can at least get some qualitative insight, which could stimulate more advanced future studies.

Within a qualitative framework for treating the correlation effects we can describe the Coulomb blockade and Kondo effects using the widely known equation of motion result (see Appendix B for more details)[37]

$$\Sigma_N^{\mathrm{QD1}}(\omega) = \omega - \varepsilon_1 - \frac{[\tilde{\omega} - \varepsilon_1]\left[\tilde{\omega} - \varepsilon_1 - U_1 - \Sigma_3^{\mathrm{QD1}}(\omega)\right] + U_1\Sigma_1^{\mathrm{QD1}}(\omega)}{\tilde{\omega} - \varepsilon_1 - \left[\Sigma_3^{\mathrm{QD1}}(\omega) + U_1(1 - \langle\hat{n}_{1\downarrow}\rangle)\right]}, \tag{8}$$

where $\Sigma_{\nu=1,3}^{\mathrm{QD1}}(\omega) = \sum_{\mathbf{k}} |V_{\mathbf{k}N}|^2 [f(\xi_{\mathbf{k}N}, T)]^{(3-\nu)/2} [(\omega - \xi_{\mathbf{k}N})^{-1} + (\omega - U_1 - 2\varepsilon_1 + \xi_{\mathbf{k}N})^{-1}]$ and $\tilde{\omega} = \omega + \frac{i\Gamma_N}{2}$. We investigated the interfacial quantum dot spectrum and the related transport properties at $k_B T = 0.001\Gamma_N$, i.e., well below the Kondo temperature. Specific numerical computations have been performed for $\varepsilon_1 = -0.75\Gamma_N$, $U_1 = 5\Gamma_N$, and for symmetric coupling to both external leads, which guarantees the optimal conditions for observing any low-bias features in the Andreev current.[5,16] The ratio $\Gamma_S/\Gamma_N \sim 1$ is a reason why the particle-hole splitting is hardly visible, but otherwise (for larger Γ_S) the Kondo peak is either reduced or completely absent.[16]

The upper panel in Fig. 6 illustrates the Fano resonance/antiresonance around $\pm\varepsilon_2$ (where $\varepsilon_2 = 0.25\Gamma_N$) obtained for the hopping $t = 0.1\Gamma_N$. These Fano-type interference objects appear on top of the characteristic spectrum consisting of the Kondo resonance and the broad quasiparticle peaks seen at ε_1 and its Coulomb satellite at $\varepsilon_1 + U_1$. Such a spectrum is a combined result of the interference effects discussed in the preceding section and the correlation features. The lower panel of Fig. 6 corresponds to the very specific situation $\varepsilon_2 = 0$, when the Kondo and Fano structures happen to coincide. Fano-type resonance then turns out to play a dominant role.

Differential conductance of the Andreev current (4) for the T-shaped double quantum dot system (1) is shown in Fig. 7. We notice a clear suppression of the zero-bias peak (for the single quantum dot case $t = 0$ indicated by the dashed lines) because of a destructive influence of the Fano-type interference (the solid lines). The subgap Andreev current is thus very sensitive to the interplay between the Kondo and Fano effects.

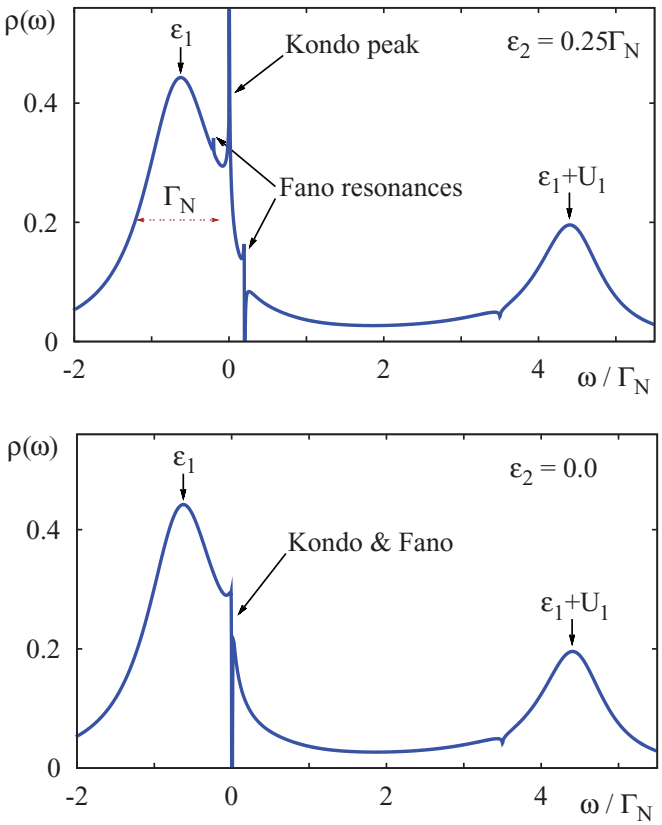

FIG. 6. (Color online) Density of states $\rho(\omega)$ of the correlated interfacial QD in the Kondo regime obtained for $\varepsilon_1 = -0.75\Gamma_N$, $\Gamma_S = \Gamma_N$, $U = 5\Gamma_N$, $t = 0.1\Gamma_N$, and temperature $k_BT = 0.001\Gamma_N$. The upper panel shows the spectrum for $\varepsilon_2 = 0.25\Gamma_N$ with two Fano structures appearing at $\pm\varepsilon_2$ aside the Kondo peak. The lower plot corresponds to $\varepsilon_2 = 0$ when both the Kondo and Fano structures are superimposed.

For obvious reasons their most dramatic competition occurs when energy of the side-coupled quantum dot coincides with the Kondo resonance, i.e., for $\varepsilon_2 = 0$. Quantum interference effects then destroy the Kondo peak washing out the zero-bias enhancement of the Andreev conductance.

V. INFLUENCE OF INTERACTIONS U_2

Coulomb interactions U_2 at the side-coupled quantum dot can have additional effects on the transport properties of the T-shape heterojunction shown in Fig. 1. At low temperatures in the subgap regime $|eV| < \Delta$ the current comes solely from the Andreev channel, so the correlations U_2 (indirectly) affect the transmittance $T_A(\omega) = \Gamma_N^2 |G_{1,12}(\omega)|^2$ through the Green's function $\boldsymbol{G}_1(\omega)$ of the interfacial quantum dot.

To study the influence of such correlations U_2 we use the following (exact for $U_1 = 0$) relation:

$$\boldsymbol{\Sigma}_1^0(\omega) = \begin{pmatrix} -\frac{i\Gamma_N}{2} & -\frac{\Gamma_S}{2} \\ -\frac{\Gamma_S}{2} & -\frac{i\Gamma_N}{2} \end{pmatrix} + |t|^2 \boldsymbol{G}_2(\omega), \tag{9}$$

where $\boldsymbol{G}_2(\omega)$ is the Fourier transform of the single-particle Green's function $\boldsymbol{G}_2(t',t_0) = -i\hat{T}\langle \hat{\Psi}_2(t')\hat{\Psi}_2^\dagger(t_0)\rangle$ for the side-coupled quantum dot with the standard Nambu spinors $\hat{\Psi}_2^\dagger = (\hat{d}_{2\uparrow}^\dagger, \hat{d}_{2\downarrow})$ and $\hat{\Psi}_2 = (\hat{\Psi}_2^\dagger)^\dagger$. In particular, for the noninteracting case $U_2 = 0$ the Green's function $\boldsymbol{G}_2(\omega)$ simplifies[40] to the bare propagator $\boldsymbol{g}_2(\omega)$,

$$\boldsymbol{g}_2(\omega) = \begin{pmatrix} \frac{1}{\omega-\varepsilon_2} & 0 \\ 0 & \frac{1}{\omega+\varepsilon_2} \end{pmatrix}, \tag{10}$$

when Eq. (9) yields the self-energy (6) considered in Sec. III.

To explore the effects of correlations U_2 we again adopt the approximate treatment discussed in Sec. IV (with technicalities outlined in Appendix B). Upon neglecting the influence of U_2 on the proximity effect induced at the $i = 2$ quantum dot the single-particle Green's function $\boldsymbol{G}_2(\omega)$ can be determined from

$$[\boldsymbol{G}_2(\omega)]^{-1} \simeq [\boldsymbol{g}_2(\omega)]^{-1} - \begin{pmatrix} \Sigma_N^{\mathrm{QD2}}(\omega) & 0 \\ 0 & -\left[\Sigma_N^{\mathrm{QD2}}(-\omega)\right]^* \end{pmatrix}. \tag{11}$$

In analogy to Eq. (8) we now have

$$\Sigma_N^{\mathrm{QD2}}(\omega) = \omega - \varepsilon_2 - \frac{\left[\omega - \varepsilon_2 - \Sigma_0^{\mathrm{QD2}}(\omega)\right]\left[\omega - \varepsilon_2 - U_2 - \Sigma_0^{\mathrm{QD2}}(\omega) - \Sigma_3^{\mathrm{QD2}}(\omega)\right] + U_2\Sigma_1^{\mathrm{QD2}}(\omega)}{\omega - \varepsilon_2 - \Sigma_0^{\mathrm{QD2}}(\omega) - \Sigma_3^{\mathrm{QD2}}(\omega) - U_2(1 - \langle \hat{n}_{2\downarrow}\rangle)}, \tag{12}$$

with

$$\Sigma_{\nu=1,3}^{\mathrm{QD2}}(\omega) = |t|^2 \langle \hat{n}_{1\downarrow}\rangle^{(3-\nu)/2} \left(\frac{1}{\omega - \varepsilon_1} + \frac{1}{\omega + \varepsilon_1 - 2\varepsilon_2 - U_2}\right) \tag{13}$$

and $\Sigma_0^{\mathrm{QD2}}(\omega) = \frac{t^2}{\omega-\varepsilon_2}$. For vanishing U_2 Eqs. (10) and (12) properly reproduce the previous formula (6).

To have a clear indication of the new effects caused by the Coulomb interactions U_2 on the side-coupled quantum dot we focused on the case $U_1 = 0$. The top panel of Fig. 8 shows an effective spectrum of the interfacial quantum dot determined in the equilibrium situation for $U_2/\Gamma_N = 1$ and the same values of other parameters as used in Sec. III, $\varepsilon_1 = 0$, $\varepsilon_2/\Gamma_N = 0.3$, and $t/\Gamma_N = 0.2$. We can notice signatures of the charging effect caused by the Coulomb repulsion U_2. For this N-DQD-S setup we observe that besides the usual feature at $\omega = \varepsilon_2 + U_2$, an additional structure appears at $\omega = -(\varepsilon_2 + U_2)$. The latter one is strictly related to the particle-hole mixing due to the on-dot pairing.

These charging effect structures also show up in the transport properties. The differential Andreev conductance $G_A(V)$ reveals the Fano-type line shapes nearby the following characteristic values of the bias voltage: $eV = \pm\varepsilon_2$ (see Fig. 4)

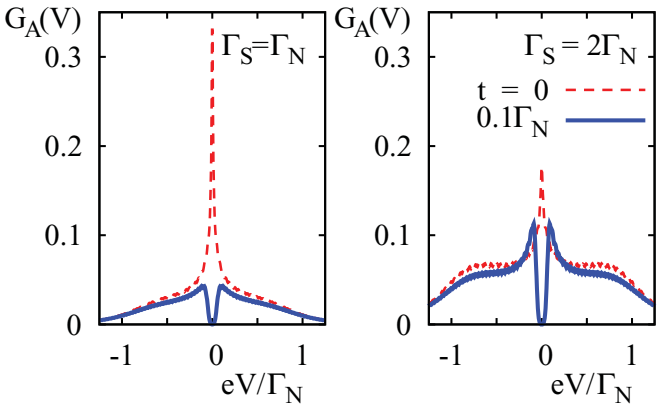

FIG. 7. (Color online) Andreev conductance $G_A(V)$ expressed in units of $4e^2/h$ obtained for $\Gamma_S = \Gamma_N$ (left panel) and $\Gamma_S = 2\Gamma_N$ (right panel). The thin dashed lines correspond to $t = 0$, whereas the thick solid lines show the influence of the Fano-type interference for $t = 0.1\Gamma_N$. In both plots we used $\varepsilon_2 = 0$ and the same model parameters as in Fig. 6.

and $eV = \pm(\varepsilon_2 + U_2)$ as shown in the lower panel of Fig. 8. We furthermore conclude that for arbitrary values of U_i the zero-bias enhancement shall be suppressed whenever the Fano-type structures $\pm\varepsilon_2$ and $\pm(\varepsilon_2 + U_2)$ coincide with the Kondo resonance of the interfacial quantum dot. An eventual possibility of the Kondo resonance formed on the side-coupled quantum dot requires a more careful investigation going beyond the level of approximation (12).

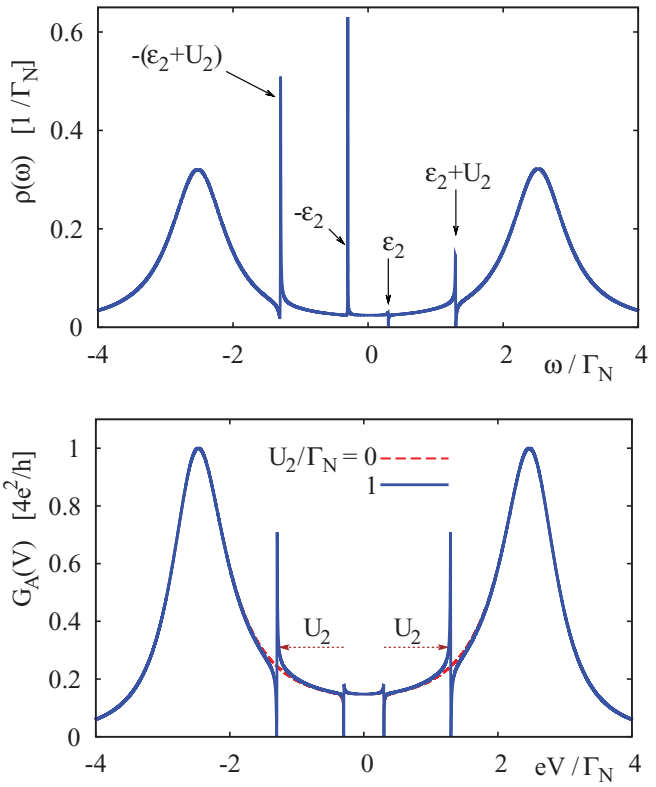

FIG. 8. (Color online) The density of states $\rho(\omega)$ of the interfacial quantum dot (top panel) and the Andreev conductance (bottom panel) obtained for the same set of parameters as in Fig. 2 with $U_2 = \Gamma_N$.

VI. SUMMARY

We have studied a unique nature in which Fano-type quantum interference manifests itself in the energy spectrum and differential conductance of the heterojunction where a metallic lead is coupled via double quantum dot to superconducting electrode. In the regime of subgap source-drain voltage $|eV| < \Delta$ the nonequilibrium charge transport is contributed only through the anomalous Andreev channel when an electron from the metallic electrode is converted into the Cooper pair (propagating further in superconductor) with a simultaneous reflection of hole back to the metallic lead. Transmittance of such Andreev scattering is a sensitive probe of the proximity-induced on-dot pairing as well as the quantum interference and the correlation effects.

Since on-dot pairing mixes the particle with hole states the interference effects are doubled in comparison to similar junctions without the superconducting electrode. In particular, for the T-shape configuration schematically shown in Fig. 1 we notice that an effective spectrum of the interfacial quantum dot develops the resonance or antiresonance at $\pm\varepsilon_2$ and $\pm(\varepsilon_2 + U_2)$. These Fano-type structures are present whenever the hopping integral t to the side-attached quantum dot ($i = 2$) is much smaller than the line-broadening Γ_N (whereas Γ_S merely controls the induced quasiparticle splitting). Upon increasing t the Fano-type features disappear, evolving into the new quasiparticle peaks (Fig. 3) being a consequence of the proximity effect indirectly spread onto the side-attached quantum dot.

The correlation effects U_1 play an important role with regard to the following aspects: (a) the charging effect (which causes the appearance of the Coulomb satellite near $\varepsilon_1 + U_1$), (b) the Kondo singlet state (when the interfacial quantum dot spin is effectively screened by electrons of the metallic electrode) leading to formation of a narrow resonance at μ_N, and (c) eventual suppression of the on-dot pairing (not studied here). We have previously shown[16] that the Kondo effect can enhance the zero-bias Andreev conductance as confirmed experimentally.[5] In the present work we indicate that in the double quantum dots the quantum interference can (destructively) affect such enhancement whenever the Fano-type structures appear nearby the Kondo peak.

A more detailed analysis of the Fano-Kondo interplay could be a challenging task for future studies. For this purpose one should resort to either nonperturbative techniques, such as the numerical renormalization group, or to the sophisticated perturbative methods capable of interpolation between the limits $t \to 0$, $\Gamma_\beta \to 0$, and $U \to 0$.

ACKNOWLEDGMENTS

We thank B. Bułka and K. I. Wysokiński for instructive discussions on the Fano resonances in nanophysics. This work is partly supported by the Polish Ministry of Science and Education under Grant No. NN202187833.

APPENDIX A: SELF-ENERGY OF THE NONCORRELATED DQD

Using the standard Nambu notation we can express the retarded Green's functions of the metallic lead

$$\boldsymbol{g}_N(\mathbf{k},\omega) = \begin{pmatrix} \frac{1}{\omega-\xi_{\mathbf{k}N}} & 0 \\ 0 & \frac{1}{\omega+\xi_{\mathbf{k}N}} \end{pmatrix}, \tag{A1}$$

the (unperturbed) side-attached quantum dot

$$\boldsymbol{g}_2(\omega) = \begin{pmatrix} \frac{1}{\omega-\varepsilon_2} & 0 \\ 0 & \frac{1}{\omega+\varepsilon_2} \end{pmatrix}, \tag{A2}$$

and the isotropic superconductor

$$\boldsymbol{g}_S(\mathbf{k},\omega) = \begin{pmatrix} \frac{u_{\mathbf{k}}^2}{\omega-E_{\mathbf{k}}} + \frac{v_{\mathbf{k}}^2}{\omega+E_{\mathbf{k}}} & \frac{-u_{\mathbf{k}}v_{\mathbf{k}}}{\omega-E_{\mathbf{k}}} + \frac{u_{\mathbf{k}}v_{\mathbf{k}}}{\omega+E_{\mathbf{k}}} \\ \frac{-u_{\mathbf{k}}v_{\mathbf{k}}}{\omega-E_{\mathbf{k}}} + \frac{u_{\mathbf{k}}v_{\mathbf{k}}}{\omega+E_{\mathbf{k}}} & \frac{u_{\mathbf{k}}^2}{\omega+E_{\mathbf{k}}} + \frac{v_{\mathbf{k}}^2}{\omega-E_{\mathbf{k}}} \end{pmatrix}. \tag{A3}$$

In Eq. (A3) we applied the BCS coefficients

$$u_{\mathbf{k}}^2, v_{\mathbf{k}}^2 = \frac{1}{2}\left[1 \pm \frac{\xi_{\mathbf{k}S}}{E_{\mathbf{k}}}\right],$$
$$u_{\mathbf{k}}v_{\mathbf{k}} = \frac{\Delta}{2E_{\mathbf{k}}},$$

where $E_{\mathbf{k}} = \sqrt{\xi_{\mathbf{k}S}^2+\Delta^2}$.

For the case of uncorrelated quantum dots ($U_i = 0$) we can determine the self-energy $\Sigma^0(\omega)$ of the interfacial quantum dot from the following equation:

$$\boldsymbol{\Sigma}^0(\omega) = \sum_{\mathbf{k},\beta=N,S} V_{\mathbf{k}\beta}\boldsymbol{g}_\beta(\mathbf{k},\omega)V_{\mathbf{k}\beta}^* + t\,\boldsymbol{g}_2(\omega)t^*. \tag{A4}$$

Assuming the wide-band limit we introduce the constant weighted density of states

$$2\pi\sum|V_{\mathbf{k}\beta}|^2\delta(\omega-\xi_{\mathbf{k},\beta}) = \begin{cases}\Gamma_\beta & \text{for} \quad |\xi_{\mathbf{k},\beta}| < D/2 \\ 0 & \text{elsewhere,}\end{cases} \tag{A5}$$

where D is the conduction bandwidth. We then find that

$$\sum_{\mathbf{k}} V_{\mathbf{k}N}\boldsymbol{g}_N(\mathbf{k},\omega)V_{\mathbf{k}N}^* = \begin{pmatrix} \frac{-i\Gamma_N}{2} & 0 \\ 0 & \frac{-i\Gamma_N}{2} \end{pmatrix} \tag{A6}$$

because, according to the Kramers-Krönig relation, the real part disappears. In the same way, we find from straightforward algebra that[2]

$$\sum_{\mathbf{k}} V_{\mathbf{k}S}\boldsymbol{g}_S(\mathbf{k},\omega)V_{\mathbf{k}S}^* = \frac{\gamma(\omega)\Gamma_S}{2i}\begin{pmatrix} -1 & \frac{\Delta}{\omega} \\ \frac{\Delta}{\omega} & -1 \end{pmatrix}, \tag{A7}$$

where

$$\gamma(\omega) = \frac{|\omega|\,\Theta(|\omega|-\Delta)}{\sqrt{\omega^2-\Delta^2}} - \frac{i\omega\,\Theta(\Delta-|\omega|)}{\sqrt{\Delta^2-\omega^2}}. \tag{A8}$$

In the extreme subgap limit $|\omega| \ll \Delta$ the function (A8) approaches $\gamma(\omega) \to -i\omega/\Delta$, so in consequence

$$\lim_{|\omega|\ll\Delta}\boldsymbol{\Sigma}^0(\omega) = \begin{pmatrix} \frac{-i\Gamma_N}{2} + \frac{|t|^2}{\omega-\varepsilon_2} & \frac{-\Gamma_S}{2} \\ \frac{-\Gamma_S}{2} & \frac{-i\Gamma_N}{2} + \frac{|t|^2}{\omega+\varepsilon_2} \end{pmatrix}, \tag{A9}$$

which proves Eq. (6).

APPENDIX B: DETERMINATION OF $\Sigma_N(\omega)$

In this appendix we recollect the main steps leading to the derivation of the self-energy $\Sigma_N(\omega)$ expressed in Eq. (8). To focus on the correlation effects caused by U_1 (in the normal channel) for the deep subgap regime $|\omega| \ll \Delta$ we restrict ourselves to the equilibrium situation $\mu_N = \mu_S$ and identical temperatures T_β. Under such conditions the Green's functions $-i\hat{T}\langle\hat{A}(t')\hat{B}(t_0)\rangle$ depend on the time difference $t'-t_0$, so for convenience we can set $t_0 = 0$.

We shall determine the single-particle Green's function $G_1(t) = -i\hat{T}\langle\hat{d}_{1\uparrow}(t)\hat{d}_{1\uparrow}^\dagger\rangle$ (we no longer use the matrix Nambu notation in this appendix). Fourier transform of the single-particle Green's function can be written as

$$G_1(\omega) = [\omega - \varepsilon_1 - \Sigma_N(\omega)]^{-1}, \tag{B1}$$

where the self-energy $\Sigma_N(\omega)$ accounts for both the hybridization to the external electrodes and for the on-dot correlations. In the subgap regime the hybridization to superconducting lead is not efficient (due to lack of any in-gap states in the superconductor), therefore the self-energy for the noninteracting case $U_1 = 0$ is simply given by $\Sigma_0(\omega) = \sum_{\mathbf{k}}\frac{|V_{\mathbf{k}N}|^2}{\omega-\xi_{\mathbf{k}N}}$ as discussed in Appendix A.

We now consider the correlation effects, determining the self-energy $\Sigma_N(\omega)$ from the equation of motion scheme.[37] Applying it to the single-particle Green's function $G_1(\omega)$ we obtain the following (exact) relation:

$$G_1(\omega) = g_1(\omega) + g_1(\omega)U_1G_1^{(2)}(\omega), \tag{B2}$$

where $g_1(\omega) = [\omega - \varepsilon_1 - \Sigma_0(\omega)]^{-1}$ denotes the noninteracting propagator and the higher-order Green's function is defined as $G_1^{(2)}(t) = -i\hat{T}\langle\hat{d}_{1\uparrow}(t)\hat{n}_{1\downarrow}(t)\hat{d}_{1\uparrow}^\dagger\rangle$. The equation of motion for such Green's function $G_1^{(2)}$,

$$\begin{aligned}(\omega-\varepsilon_1-U_1)\,G_1^{(2)}(\omega) \\ = \langle\hat{n}_{1\downarrow}\rangle + \sum_{\mathbf{q}}\left[V_{\mathbf{q}N}^*\Gamma_{\mathbf{q}N}^{(1)}(\omega) + V_{\mathbf{q}N}\Gamma_{\mathbf{q}N}^{(2)}(\omega) - V_{\mathbf{q}N}^*\Gamma_{\mathbf{q}N}^{(3)}(\omega)\right],\end{aligned} \tag{B3}$$

introduces the mixed Green's functions

$$\Gamma_{\mathbf{q}N}^{(1)}(t) = -i\hat{T}\langle\hat{c}_{\mathbf{q}\uparrow N}(t)\hat{n}_{1\downarrow}(t)\hat{d}_{1\uparrow}^\dagger\rangle, \tag{B4}$$

$$\Gamma_{\mathbf{q}N}^{(2)}(t) = -i\hat{T}\langle\hat{c}_{\mathbf{q}\downarrow N}^\dagger(t)\hat{d}_{1\uparrow}(t)\hat{d}_{1\downarrow}(t)\hat{d}_{1\uparrow}^\dagger\rangle, \tag{B5}$$

$$\Gamma_{\mathbf{q}N}^{(3)}(t) = -i\hat{T}\langle\hat{c}_{\mathbf{q}\downarrow N}(t)\hat{d}_{1\downarrow}^\dagger(t)\hat{d}_{1\downarrow}(t)\hat{d}_{1\uparrow}^\dagger\rangle. \tag{B6}$$

Upon computing the equations of motions for each of the mixed Green's functions (B4)–(B6) we again encounter the following class of higher-order Green's functions $-i\hat{T}\langle\hat{c}_{\mathbf{q}\sigma_1 N}^{(\dagger)}(t)\hat{c}_{\mathbf{k}\sigma_2 N}^{(\dagger)}(t)\hat{d}_{1\sigma_3}^{(\dagger)}(t)\hat{d}_{1\uparrow}^\dagger\rangle$. In order to truncate these equations we neglect the propagators corresponding to different spins,

$$-i\hat{T}\langle\hat{c}_{\mathbf{q}\uparrow N}(t)\hat{c}_{\mathbf{k}\downarrow N}^\dagger(t)\hat{d}_{1\downarrow}(t)\hat{d}_{1\uparrow}^\dagger\rangle \simeq 0,$$
$$-i\hat{T}\langle\hat{c}_{\mathbf{q}\uparrow N}(t)\hat{c}_{\mathbf{k}\downarrow N}(t)\hat{d}_{1\uparrow}^\dagger(t)\hat{d}_{1\uparrow}^\dagger\rangle \simeq 0,$$
$$-i\hat{T}\langle\hat{c}_{\mathbf{q}\downarrow N}^\dagger(t)\hat{c}_{\mathbf{k}\uparrow N}(t)\hat{d}_{1\downarrow}(t)\hat{d}_{1\uparrow}^\dagger\rangle \simeq 0,$$
$$-i\hat{T}\langle\hat{c}_{\mathbf{q}\downarrow N}(t)\hat{c}_{\mathbf{k}\uparrow N}(t)\hat{d}_{1\downarrow}^\dagger(t)\hat{d}_{1\uparrow}^\dagger\rangle \simeq 0,$$

while for identical spins we impose the linearizations

$$-i\hat{T}\langle\hat{c}^{\dagger}_{\mathbf{q}\downarrow N}(t)\hat{c}_{\mathbf{k}\downarrow N}(t)\hat{d}_{1\uparrow}(t)\hat{d}^{\dagger}_{1\uparrow}\rangle \simeq \delta_{\mathbf{k},\mathbf{q}} f(\xi_{\mathbf{q}N})G_1(t),$$
$$-i\hat{T}\langle\hat{c}_{\mathbf{q}\downarrow N}(t)\hat{c}^{\dagger}_{\mathbf{k}\downarrow N}(t)\hat{d}_{1\uparrow}(t)\hat{d}^{\dagger}_{1\uparrow}\rangle \simeq \delta_{\mathbf{k},\mathbf{q}} f(-\xi_{\mathbf{q}N})G_1(t).$$

With such approximations the set of coupled equations for the Green's functions (B4)–(B6) become closed. At this level we thus obtain

$$\Gamma^{(1)}_{\mathbf{q}N}(\omega) \simeq \frac{V_{\mathbf{q}N}}{(\omega - \xi_{\mathbf{q}N})}, \tag{B7}$$

$$\Gamma^{(2)}_{\mathbf{q}N}(\omega) \simeq V^{*}_{\mathbf{q}N}\frac{G^{(2)}_1(\omega) - f(\xi_{\mathbf{q}N})G_1(\omega)}{\omega + \xi_{\mathbf{q}N} - 2\varepsilon_1 - U_1}, \tag{B8}$$

$$\Gamma^{(3)}_{\mathbf{q}N}(\omega) \simeq -V_{\mathbf{q}N}\frac{G^{(2)}_1(\omega) - f(\xi_{\mathbf{q}N})G_1(\omega)}{\omega - \xi_{\mathbf{q}N}}. \tag{B9}$$

Substituting Eqs. (B7)–(B9) for Eq. (B3) we get

$$G^{(2)}_1(\omega) \simeq \frac{\langle\hat{n}_{1\downarrow}\rangle - \Sigma_1(\omega)G_1(\omega)}{\omega - \varepsilon_1 - \Sigma_0(\omega) - U_1 - \Sigma_3(\omega)}, \tag{B10}$$

where

$$\Sigma_\nu(\omega) = \sum_{\mathbf{q}}[f(\xi_{\mathbf{q}N})]^{(3-\nu)/2}|V_{\mathbf{q}N}|^2 \times\left[\frac{1}{\omega - \xi_{\mathbf{q}N}} + \frac{1}{\omega + \xi_{\mathbf{q}N} - 2\varepsilon_1 - U_1}\right]. \tag{B11}$$

Combining Eq. (B10) with the exact relation (B2) finally reproduces the result originally proposed in Ref. 41:

$$G_1(\omega) \simeq \frac{g_1^{-1}(\omega) - \Sigma_3(\omega) - (1 - \langle\hat{n}_{1\downarrow}\rangle)U_1}{g_1^{-1}(\omega)[g_1^{-1}(\omega) - U_1 - \Sigma_3(\omega)] + U_1\Sigma_1(\omega)}. \tag{B12}$$

Through the Dyson equation (B1) this yields the self-energy $\Sigma_N(\omega)$ used in Eq. (8), where the noninteracting propagator in the wide bandwidth limit is simplified to $g_1(\omega) = [\tilde{\omega} - \varepsilon_1]^{-1}$ with $\tilde{\omega} \equiv \omega + i\Gamma_N/2$.

[1] M. Pustilnik and L. I. Glazman, J. Phys.: Condens. Matter **16**, R513 (2004).

[2] Y. Yamada, Y. Tanaka, and N. Kawakami, Phys. Rev. B **84**, 075484 (2011).

[3] P. W. Anderson, P. A. Lee, M. Randeria, T. M. Rice, N. Trivedi, and F. C. Zhang, J. Phys.: Condens. Matter **16**, R755 (2004).

[4] Y. V. Nazarov and Y. L. Blanter, *Quantum Transport: Introduction to Nanosciene* (Cambridge University Press, Cambridge, 2009).

[5] R. S. Deacon, Y. Tanaka, A. Oiwa, R. Sakano, K. Yoshida, K. Shibata, K. Hirakawa, and S. Tarucha, Phys. Rev. Lett. **104**, 076805 (2010); Phys. Rev. B **81**, 121308(R) (2010), and the Supplemental Material on-line information.

[6] R. Fazio and R. Raimondi, Phys. Rev. Lett. **80**, 2913 (1998); **82**, 4950 (1999); P. Schwab and R. Raimondi, Phys. Rev. B **59**, 1637 (1999).

[7] A. A. Clerk, V. Ambegaokar, and S. Hershfield, Phys. Rev. B **61**, 3555 (2000).

[8] J. C. Cuevas, A. Levy Yeyati, and A. Martin-Rodero, Phys. Rev. B **63**, 094515 (2001).

[9] M. Krawiec and K. I. Wysokiński, Supercond. Sci. Technol. **17**, 103 (2004).

[10] Y. Tanaka, N. Kawakami, and A. Oguri, J. Phys. Soc. Jpn. **76**, 074701 (2007).

[11] J. Bauer, A. Oguri, and A. C. Hewson, J. Phys.: Condens. Matter **19**, 486211 (2007).

[12] T. Hecht, A. Weichselbaum, J. von Delft, and R. Bulla, J. Phys.: Condens. Matter **20**, 275213 (2008).

[13] Q.-F. Sun, J. Wang, and T.-H. Lin, Phys. Rev. B **59**, 3831 (1999); Q.-F. Sun, H. Guo, and T.-H. Lin, Phys. Rev. Lett. **87**, 176601 (2001).

[14] S. Y. Cho, K. Kang, and C.-M. Ryu, Phys. Rev. B **60**, 16874 (1999).

[15] Y. Avishai, A. Golub, and A. D. Zaikin, Phys. Rev. B **63**, 134515 (2001); T. Aono, A. Golub, and Y. Avishai, *ibid.* **68**, 045312 (2003).

[16] T. Domański and A. Donabidowicz, Phys. Rev. B **78**, 073105 (2008); T. Domański, A. Donabidowicz, and K. I. Wysokiński, *ibid.* **78**, 144515 (2008); **76**, 104514 (2007).

[17] V. Koerting, B. M. Andersen, K. Flensberg, and J. Paaske, Phys. Rev. B **82**, 245108 (2010).

[18] M. R. Graeber, T. Nussbaumer, W. Belzig, and C. Schönenberger, Nanotechnology **15**, 479 (2004).

[19] L. Hofstetter, A. Geresdi, M. Aagesen J. Nygard, C. Schönenberger, and S. Csonka, Phys. Rev. Lett. **104**, 246804 (2010).

[20] L. G. Herrmann, F. Portier, P. Roche, A. L. Yeyati, T. Kontos, and C. Strunk, Phys. Rev. Lett. **104**, 026801 (2010).

[21] J. Eldridge, M. G. Pala, M. Governale, and J. König, Phys. Rev. B **82**, 184507 (2010).

[22] B. Sothmann, D. Futterer, M. Governale, and J. König, Phys. Rev. B **82**, 094514 (2010).

[23] Y. Yamada, Y. Tanaka, and N. Kawakami, J. Phys. Soc. Jpn. **79**, 043705 (2010).

[24] J.-D. Pillet, C. H. L. Quay, P. Morfin, C. Bena, A. Levy-Yeyati, and P. Joyez, Nat. Phys. **6**, 965 (2010).

[25] A. E. Miroshnichenko, S. Flach, and Y. S. Kivshar, Rev. Mod. Phys. **82**, 2257 (2010).

[26] Y. Tanaka, N. Kawakami, and A. Oguri, Phys. Rev. B **78**, 035444 (2008); J. Phys.: Conf. Series **150**, 022086 (2009).

[27] Y. Tanaka, N. Kawakami, and A. Oguri, Phys. Rev. B **81**, 075404 (2010).

[28] W. Hofstetter, J. König, and H. Schoeller, Phys. Rev. Lett. **87**, 156803 (2001).

[29] B. R. Bułka and P. Stefański, Phys. Rev. Lett. **86**, 5128 (2001).

[30] N. Knorr, M. A. Schneider, L. Diekhöner, P. Wahl, and K. Kern, Phys. Rev. Lett. **88**, 096804 (2002).

[31] V. Madhavan, W. Chen, T. Jamneala, M. F. Crommie, and N. S. Wingreen, Phys. Rev. B **64**, 165412 (2001).

[32] A. A. Aligia and A. M. Lobos, J. Phys.: Condens. Matter **17**, S1095 (2005).
[33] J. Figgins and D. K. Morr, Phys. Rev. Lett. **104**, 187202 (2010).
[34] R. Žitko, Phys. Rev. B **81**, 115316 (2010).
[35] P. Trocha and J. Barnaś, Phys. Rev. B **76**, 165432 (2007).
[36] T. Meng, S. Florens, and P. Simon, Phys. Rev. B **79**, 224521 (2009).
[37] H. Haug and A.-P. Jauho, *Quantum Kinetics in Transport and Optics of Semiconductors* (Springer-Verlag, Berlin, 1996).
[38] S. Sasaki, H. Tamura, T. Akazaki, and T. Fujisawa, Phys. Rev. Lett. **103**, 266806 (2009).
[39] A. Kormanyos, I. Grace, and C. J. Lambert, Phys. Rev. B **79**, 075119 (2009).
[40] For the noninteracting case $U_i = 0$ the Green's function is formally given by $[\boldsymbol{G}_2(\omega)]^{-1} = \left[\boldsymbol{g}_2(\omega)\right]^{-1} - t^2\boldsymbol{G}_1(\omega)$, where the nonvanishing off-diagonal terms are responsible for the proximity effect on the side-coupled quantum dot. Influence of the correction $t^2\boldsymbol{G}_1(\omega)$ back on $\boldsymbol{\Sigma}_1(\omega)$ via Eq. (9) is, however, expected to be rather negligible.
[41] Y. Meir, N. S. Wingreen, and P. A. Lee, Phys. Rev. Lett. **66**, 3048 (1991).